Interference phenomena at backscattering by ice crystals of cirrus clouds

Anatoli Borovoi,[1,2,*] Natalia Kustova,[1] and Alexander Konoshonkin[1,2]

[1]*V. E. Zuev Institute of Atmospheric Optics, Rus. Acad. Sci., 1 Academician Zuev Sq., Tomsk 634021, Russia*
[2]*National Research Tomsk State University, Lenina str. 36, Tomsk 634050, Russia*
[*]*borovoi@iao.ru*

Abstract: It is shown that light backscattering by hexagonal ice crystals of cirrus clouds is formed within the physical-optics approximation by both diffraction and interference phenomena. Diffraction determines the angular width of the backscattering peak and interference produces the interference rings inside the peak. By use of a simple model for distortion of the pristine hexagonal shape, we show that the shape distortion leads to both oscillations of the scattering (Mueller) matrix within the backscattering peak and to a strong increase of the depolarization, color, and lidar ratios needed for interpretation of lidar signals.

OCIS codes: (010.1350) Backscattering; (010.1615) Clouds; (010.3640) Lidar.

References and links

1. M. I. Mishchenko, J. W. Hovenier, and L. D. Travis, *Light Scattering by Nonspherical Particles* (Academic, 2000).
2. J. C. Liu, L. Bi, R. L. Panetta, P. Yang, and M. A. Yurkin, "Comparison between the pseudo-spectral time domain method and the discrete dipole approximation for light scattering simulations," Opt. Express **20**(15), 16763–16776 (2012).
3. L. Bi and P. Yang, "Accurate simulation of the optical properties of atmospheric ice crystals with the invariant imbedding T-matrix method," J. Quant. Spectrosc. Radiat. Transf. **138**, 17–35 (2014).
4. A. G. Borovoi, N. V. Kustova, and U. G. Oppel, "Light backscattering by hexagonal ice crystal particles in the geometrical optics approximation," Opt. Eng. **44**(7), 071208 (2005).
5. A. G. Borovoi and I. A. Grishin, "Scattering matrices for large ice crystal particles," J. Opt. Soc. Am. A **20**(11), 2071–2080 (2003).
6. A. Borovoi, A. Konoshonkin, and N. Kustova, "The physical-optics approximation and its application to light backscattering by hexagonal ice crystals," J. Quant. Spectrosc. Radiat. Transf. **146**, 181–189 (2014).
7. V. Shcherbakov, J.-F. Gayet, B. Baker, and P. Lawson, "Light scattering by single natural ice crystals," J. Atmos. Sci. **63**(5), 1513–1525 (2006).
8. Z. Ulanowski, E. Hesse, P. H. Kaye, and A. J. Baran, "Light scattering by complex ice-analogue crystals," J. Quant. Spectrosc. Radiat. Transf. **100**(1-3), 382–392 (2006).
9. A. J. Baran, "A review of the light scattering properties of cirrus," J. Quant. Spectrosc. Radiat. Transf. **110**(14-16), 1239–1260 (2009).
10. B. H. Cole, P. Yang, B. A. Baum, J. Riedi, and L. C. Labonnote, "Ice particle habit and surface roughness derived from PARASOL polarization measurements," Atmos. Chem. Phys. **14**(7), 3739–3750 (2014).
11. A. Macke, J. Mueller, and E. Raschke, "Single scattering properties of atmospheric ice crystals," J. Atmos. Sci. **53**(19), 2813–2825 (1996).
12. C. Liu, R. L. Panetta, and P. Yang, "The effects of surface roughness on the scattering properties of hexagonal columns with sizes from the Rayleigh to the geometric optics regimes," J. Quant. Spectrosc. Radiat. Transf. **129**, 169–185 (2013).
13. C. Liu, R. L. Panetta, and P. Yang, "The effective equivalence of geometric irregularity and surface roughness in determining particle single-scattering properties," Opt. Express **22**(19), 23620–23627 (2014).
14. K. Sassen and S. Benson, "A midlatitude cirrus cloud climatology from the Facility for Atmospheric Remote Sensing. Part II: Microphysical properties derived from lidar depolarization," J. Atmos. Sci. **58**(15), 2103–2112 (2001).
15. W.-N. Chen, C.-W. Chiang, and J.-B. Nee, "Lidar ratio and depolarization ratio for cirrus clouds," Appl. Opt. **41**(30), 6470–6476 (2002).
16. Y. Hu, M. Vaughan, Z. Liu, B. Lin, P. Yang, D. Flittner, B. Hunt, R. Kuehn, J. Huang, D. Wu, S. Rodier, K. Powell, C. Trepte, and D. Winker, "The depolarization - attenuated backscatter relation: CALIPSO lidar measurements vs. theory," Opt. Express **15**(9), 5327–5332 (2007).
17. H. M. Cho, P. Yang, G. W. Kattawar, S. L. Nasiri, Y. Hu, P. Minnis, C. Trepte, and D. Winker, "Depolarization ratio and attenuated backscatter for nine cloud types: analyses based on collocated CALIPSO lidar and MODIS measurements," Opt. Express **16**(6), 3931–3948 (2008).

#243212 Received 17 Jun 2015; revised 30 Jul 2015; accepted 12 Aug 2015; published 10 Sep 2015

18. J. Reichardt, S. Reichardt, R.-F. Lin, M. Hess, T. J. McGee, and D. O. Starr, "Optical-microphysical cirrus model," J. Geophys. Res. **113**(D22), D22201 (2008).
19. Z. Tao, M. P. McCormick, D. Wu, Z. Liu, and M. A. Vaughan, "Measurements of cirrus cloud backscatter color ratio with a two-wavelength lidar," Appl. Opt. **47**(10), 1478–1485 (2008).
20. H. Okamoto, K. Sato, and Y. Hagihara, "Global analysis of ice microphysics from CloudSat and CALIPSO: Incorporation of specular reflection in lidar signals," J. Geophys. Res. **115**(D22), D22209 (2010).
21. Y. S. Balin, B. V. Kaul, G. P. Kokhanenko, and I. E. Penner, "Observations of specular reflective particles and layers in crystal clouds," Opt. Express **19**(7), 6209–6214 (2011).
22. K. Sassen, V. K. Kayetha, and J. Zhu, "Ice cloud depolarization for nadir and off-nadir CALIPSO measurements," Geophys. Res. Lett. **39**(20), L20805 (2012).
23. M. Hayman, S. Spuler, and B. Morley, "Polarization lidar observations of backscatter phase matrices from oriented ice crystals and rain," Opt. Express **22**(14), 16976–16990 (2014).
24. C. Zhou and P. Yang, "Backscattering peak of ice cloud particles," Opt. Express **23**(9), 11995–12003 (2015).
25. A. Borovoi, I. Grishin, E. Naats, and U. Oppel, "Backscattering peak of hexagonal ice columns and plates," Opt. Lett. **25**(18), 1388–1390 (2000).
26. A. Borovoi, A. Konoshonkin, and N. Kustova, "Backscattering by hexagonal ice crystals of cirrus clouds," Opt. Lett. **38**(15), 2881–2884 (2013).
27. A. Borovoi, A. Konoshonkin, and N. Kustova, "Backscatter ratios for arbitrary oriented hexagonal ice crystals of cirrus clouds," Opt. Lett. **39**(19), 5788–5791 (2014).
28. K. Sato and H. Okamoto, "Characterization of Ze and LDR of nonspherical and inhomogeneous ice particles for 45-GHz cloud lidar: Its implication to microphysical retrievals," J. Geophys. Res. **111**(D22), D22213 (2006).

1. Introduction

Optical and microphysical properties of cirrus clouds are needed for incorporation in up-to-date numerical models of the earth's radiance balance and, consequently, weather forecasting. At present, these properties are poorly known. Therefore considerable efforts are undertaken by both experimentalists and theorists to quantify these values. The main obstacle for theoretical calculations of optical properties of the crystals is that their sizes range from a few to hundreds micrometers. Here the standard numerical methods solving the problem of light scattering by nonspherical particles [1] are not useful since they are effective if the size parameter a, where a = (particle size)/wavelength, is less than, say, 20. Though, at present, some new methods expanding the limit of $a \le 20$ are actively developed [2,3], the results obtained are far from practical applications yet. In the case of large $a > 20$ particles, the geometric-optics approximation is reasonable. However, this approximation leads sometimes to physically inconsistent results. For example, the backscattering cross section for randomly oriented hexagonal ice crystals proves to be singular [4]. Therefore only the physical-optics approximation [5,6] is most expedient for calculating the optical properties of cirrus clouds.

While great variance of sizes, shapes, and kind of spatial orientations of the ice crystals constituting cirrus clouds make a solution of the light scattering problem to be rather complicated, a new item becomes recently a challenge for the scientific community dealing with optics of cirrus. Namely, it is suggested that ice crystal surfaces are not pristine [7–10] where imperfectness of the ice crystals is assumed to be double-natured. First, the dihedral angles inherent to the regular or pristine crystals can be slightly distorted. This case is called the shape distortion. Second, every smooth face can be imagined as a sheet of rough surface whose spatial irregularities are less than the face size. This case is called the roughened crystals. A simplest numerical method taking into account the both kinds of imperfectness was proposed by Macke within his geometric-optics or ray-tracing code [11]. Here every ray reflected or refracted by a smooth face is artificially deviated from its geometric-optics propagation direction that is just associated with the ice crystal imperfectness. A drawback of this procedure is that this approximation concerns only the light scattering process while the ice crystal surface is not explicitly determined. The ice crystal surface should be determined explicitly in any exact method based on numerical solutions of the Maxwell equations. In this way, Liu et al. [12] recently applied the PSTD (pseudo-spectral time domain) method to a roughened hexagonal column where every roughened face was simulated explicitly. However, this algorithm demands considerable computer resources and therefore it is restricted by crystals of moderate sizes. Later these authors compared the ice crystal optical properties obtained for the both models of the irregular crystals, i.e. the roughened and shape-distorted crystals, and concluded that the both models gave often similar results [13].

#243212 Received 17 Jun 2015; revised 30 Jul 2015; accepted 12 Aug 2015; published 10 Sep 2015

Among all scattering directions, the backward direction is of special importance since it is only backscattering that is detected by lidars. In spite of a long history of studying cirrus clouds by means of lidars, the problem of backscattering by ice cloud crystals has not been clarified neither experimentally nor theoretically until now [14–23]. Here the experimental data obtained from both ground-based and space-borne lidars can essentially deviate from each other because of great variance of sizes, shapes and spatial orientations of the ice crystals in the atmosphere.

In particular, in the literature there is a discussion whether there is a sharp angular peak around the backward scattering direction in cirrus clouds. To answer the question, two methods, PSTD and invariant imbedding T-matrix method (II-TM) were recently applied by Zhou and Yang to a case of a randomly oriented hexagonal column of the size parameter of $a \approx 20$ [24]. They concluded that, for this crystal, the backscattering peak appeared always independently of the crystal was regular, roughened or shape-distorted. As for the regular hexagonal crystals, we showed within the geometric-optics approximation a long time ago [25] that the backscattering peak for the regular hexagonal columns and plates always appeared owing to the corner-reflector effect. Here the dihedral angle of 90° operates as a 2D corner-reflector. Later, within the framework of the physical-optics approximation, we showed [5] that the plane-parallel beams leaving a crystal in the backward direction are scattered owing to the Fraunhofer diffraction that just results in this backscattering peak of the angular width of about $1/a$.

Meanwhile, the angular width of the backscattering peak formed by cirrus clouds is too wide to be detected by common monostatic lidars. The scattering matrix only in the center of the peak, i.e. at exactly backward direction, is needed for interpretation of lidar signals. Here such three characteristics of lidar signals as depolarization, lidar and color ratios are of practical use. These characteristics were recently calculated by the authors for the regular crystals in the cases of both random [26] and arbitrary [27] orientations. Owing to these calculations [26, 27], we were able to ascertain that the ratios calculated for the regular crystals did not match well with the available experimental data. For example, the depolarization ratio calculated for the randomly oriented hexagonal columns was equal to about 0.2 while the typical experimental data were of about 0.3 - 0.5 [14–18, 22].

In this paper, we consider the backscatter by both regular and shape-distorted hexagonal ice columns within the framework of the physical-optics approximation for the case of random orientation. Here the model for shape distortion is chosen only as a simplest geometrical one. Such a model is far from its either experimental or theoretical justifications similarly to the shape distortion model assumed in [13]. Therefore the aim of this paper is to reveal some qualitative but not quantitative regularities of the optical properties of cirrus caused by the crystal imperfectness. In particular, we emphasize that the backscatter from a regular hexagonal ice crystal is formed by both diffraction and interference phenomena where diffraction determines the angular width of the backscattering peak and interference creates the interference rings inside the peak. We show that a small distortion of the regular crystal shape damaging slightly the dihedral angle of 90° results in oscillations of the interference rings. These oscillations are largest in the center of the backscattering peak that essentially increase the depolarization ratio approaching its magnitude to the experimental values. However, a rather large shape distortion eliminates the backscattering peak.

2. Hexagonal ice columns of regular and irregular shapes

The purpose of this paper is to clarify the main physical regularities appearing in optical properties of cirrus clouds because of small deviations of crystal surfaces from their regular or pristine shapes. We choose the hexagonal column as the basic shape since it is the typical shape of the crystals in cirrus clouds. Besides, it is the hexagonal column that is used in majority of the papers dealing with any test calculations of the optical properties. In this paper, we consider the hexagonal column of the typical diameter of $D = 30\,\mu\text{m}$. Heights of the columns h in cirrus clouds are not statistically independent of the diameters. The height is

#243212 Received 17 Jun 2015; revised 30 Jul 2015; accepted 12 Aug 2015; published 10 Sep 2015

taken from the model of [28] as $h = 73.64\,\mu\text{m}$. The refractive index is taken as 1.3116 and 1.3004 for $\lambda = 0.532\,\mu\text{m}$ and $\lambda = 1.064\,\mu\text{m}$, respectively. The main axis is assumed to pass through centers of the hexagonal faces.

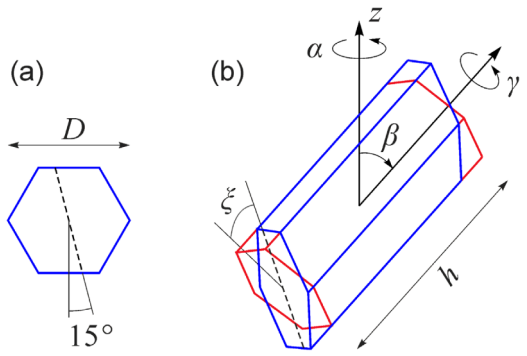

Fig. 1. Geometry of the irregular hexagonal column.

The shape distortion of the column is defined by a simultaneous tilt of the both hexagonal faces relative to the main column axis. The tilt is chosen along the dashed line depicted in Fig. 1(a). Such distortion destroys all dihedral angles of 90° inside the crystal and excludes any plane of symmetry of the particle. The angle of the tilt ξ characterizes the surface distortion and it is called the distortion angle.

Orientation of a column is determined by three Euler angles α, β, and γ shown in Fig. 1(b) where α defines rotation of the crystal about the incident direction; β is the crystal tilt, i.e. the angle between the incident direction and the main axis; and γ describes crystal rotation about the main axis.

This model of the irregular crystal shape is taken because it is the simplest scheme distorting the dihedral angle of 90° responsible for appearance of the backscattering peak. Of course, this model has neither experimental base nor any justification within the crystal physics. This model is designed only to study qualitatively the tendencies appeared in the backscattering properties when the dihedral angle of 90° is violated. Nevertheless, defending this model, we mention that the similar geometrical models are used in other papers dealing with light scattering by crystals with shape distortion (e.g [13].).

3. Scattering matrices and backscatter ratios

In general, light scattering by an arbitrary particle is completely determined by the 4×4 scattering or Mueller matrix [1]. If a particle of arbitrary shape is randomly oriented, there are pairs of the so-called reciprocal particle orientations that reduce the number of independent elements of the Mueller matrix from 16 to 10 as follows

$$\mathbf{M}(\theta) = \sigma(\theta)\begin{pmatrix} 1 & m_{12}(\theta) & m_{13}(\theta) & m_{14}(\theta) \\ m_{12}(\theta) & m_{22}(\theta) & m_{23}(\theta) & m_{24}(\theta) \\ -m_{13}(\theta) & -m_{23}(\theta) & m_{33}(\theta) & m_{34}(\theta) \\ m_{14}(\theta) & m_{24}(\theta) & -m_{34}(\theta) & m_{44}(\theta) \end{pmatrix}. \qquad (1)$$

The zenith scattering angle θ is counted, for convenience, from the backward scattering direction $\theta = 0$. In Eq. (1), the first element of the matrix $M_{11}(\theta) = \sigma(\theta)$ has a simple physical meaning of the differential scattering cross section in the case of unpolarized incident light. Other dimensionless elements of the matrix $m_{ij}(\theta)$ are responsible for light

#243212 Received 17 Jun 2015; revised 30 Jul 2015; accepted 12 Aug 2015; published 10 Sep 2015

polarization. If the particle has a plane of symmetry like the regular hexagonal column, four elements m_{13}, m_{14}, m_{23}, and m_{24} become zero.

Lidars detect only light scattered in the backward direction. For the backward direction $\theta = 0$, the matrix is simplified as

$$\mathbf{M}(0) = \sigma(0)\begin{pmatrix} 1 & 0 & 0 & m_{14}(0) \\ 0 & m_{22}(0) & 0 & 0 \\ 0 & 0 & -m_{22}(0) & 0 \\ m_{14}(0) & 0 & 0 & 1-2m_{22}(0) \end{pmatrix}. \tag{2}$$

Here we get only three independent values σ, m_{22}, and m_{14}. Moreover, the element $m_{14}(0)$ is nonzero only for the irregular columns. For the regular column, we have $m_{14} = 0$ since there is a plane of symmetry. It is worthwhile to note that the backscattering cross section of the randomly oriented particles $\sigma(0)$ is the same for both unpolarized and linearly polarized incident light according to Eq. (2).

However, lidar detectors are of finite fields of view, and the light scattered near the backward direction contributes to the lidar signals as well. Consequently, we need to know the total matrix of Eq. (1) in the vicinity of the backward direction. If the detector is circular, it can be mentally divided into ring detectors collecting the light over all azimuth angles φ at a fixed zenith angle θ. The Mueller matrix for the ring detector $\mathbf{M}_r(\theta)$ has the same symmetry as Eq. (2). It is obtained from Eq. (1) as

$$\mathbf{M}_r(\theta) = \frac{1}{2\pi}\int_0^{2\pi} \mathbf{L}(\varphi)\mathbf{M}(\theta)\mathbf{L}(\varphi)d\varphi = \\ = \sigma(\theta)\begin{pmatrix} 1 & 0 & 0 & m_{14}(\theta) \\ 0 & \mu_{22}(\theta) & 0 & 0 \\ 0 & 0 & -\mu_{22}(\theta) & 0 \\ m_{14}(\theta) & 0 & 0 & m_{44}(\theta) \end{pmatrix}, \tag{3}$$

where $\mathbf{L}(\varphi)$ is the well-known rotation matrix for the Stokes parameters and $\mu_{22}(\theta) = [m_{22}(\theta) - m_{33}(\theta)]/2$. In this case, four quantities σ, μ_{22}, m_{44}, and m_{14} are independent. For the regular column, one of them disappears: $m_{14}(\theta) = 0$.

In lidar studies, three dimensionless ratios are often used instead of the Mueller matrix. They are

$$\delta_l = \frac{\sigma_\perp(0)}{\sigma_\parallel(0)}, L = \frac{\sigma_e}{\sigma(0)}, \chi = \frac{\sigma(0,\lambda_1)}{\sigma(0,\lambda_2)}. \tag{4}$$

The quantity δ_l is the linear depolarization ratio. It is obtained when the incident light is linearly polarized and the backscattering cross section is detected with the polarizer which is either perpendicular $\sigma_\perp(0)$ or parallel $\sigma_\parallel(0)$ to the incident light. The quantity L is called either the extinction-to-backscatter or lidar ratio. Here σ_e is the extinction cross section for the randomly oriented crystals that is calculated separately. The quantity χ is the color ratio which is detected by a two-wavelength lidar.

The linear depolarization ratio is expressed through the elements of the Mueller matrix (2) as

#243212 Received 17 Jun 2015; revised 30 Jul 2015; accepted 12 Aug 2015; published 10 Sep 2015

$$\delta_l = \frac{1 - m_{22}(0)}{1 + m_{22}(0)}. \tag{5}$$

If the linear depolarization ratio was measured in the vicinity of the backward direction $\theta \neq 0$, this quantity would be dependent on orientation of the polarizer used by detector. To avoid this dependence, we use the Mueller matrix of the ring detector of Eq. (3) where orientation of a polarizer in a lidar detector is indifferent. In this case, the depolarization ratio is described by the similar equation

$$\delta_l(\theta) = \frac{1 - \mu_{22}(\theta)}{1 + \mu_{22}(\theta)}. \tag{6}$$

Equations (5) and (6) coincide in the backward direction $\theta = 0$.

4. The straight and skew corner-reflection beams at backscattering

We calculate three Mueller matrixes of Eqs. (1)-(3) numerically by use of our both geometric-optics and physical-optics codes. For the beginning, let us shortly describe the geometric-optics and physical-optics approximations. In the geometric-optics approximation [4], every illuminated crystal face splits the incident light into two plane-parallel beams. The first beam corresponds to the specular reflection by the illuminated face and the second one is the refracted beam. Then the refracted beam propagates inside the crystal until it meets one or several intersecting faces. Every new face, in its turn, splits the beam into two beams, and so on. So the scattered light leaving a crystal surface consists of a lot of plane-parallel beams propagating in different directions. Every beam is characterized by its trajectory defined by a sequence of the faces passed by the beam. Also any beam is characterized by its location on the exit face and polygonal transversal shape, as well as by intensity, phase and polarization of light.

By definition, the physical-optics approximation assumes [6] that the scattered light on particle surface is found in the geometric-optics approximation. The geometric-optics and physical-optics approximations treat differently only propagation of scattered light from the particle surface to an observation point. Usually the observation point is localized in the far or wave zone where the scattered light is determined on the scattering direction sphere as several functions of the zenith θ and azimuth φ scattering angles. In the geometric-optics approximation, every plane-parallel beam leaving a crystal is mapped to a dot on the scattering direction sphere where the dot corresponds to the propagation direction of the beam near the particle surface. Mathematically, this dot is described by the Dirac delta-function on the scattering direction sphere. In the physical-optics approximation, this dot is replaced by a spot around the geometric-optics dot that corresponds to the Fraunhofer diffraction of the beam. As known, the diffraction spot has the angular radius of λ / A where A is the transversal size of the beam.

Our previous numerical calculations performed for randomly oriented regular columns [4,5,26] proved that predominant contribution to both the backward direction $\theta = 0$ and its vicinity $\theta \neq 0$ is obtained from only eight beams shown in Fig. 2. The beams are marked by numbers in Fig. 2(a). These beams are associated with the corner-reflection effect produced by the dihedral angle of 90° between crystal faces [25]. The beams 1-4 leaving the skew rectangular faces are called the skew ones while the other beams 5-8 are called the straight ones. Here $\gamma = 0°$ denotes one of possible six angles γ where a rib at $\beta \neq 0$ becomes perpendicular to the incident direction. It is important that all the beams reveal a sharp maximum of their contributions to the backscatter if a column is orientated as ($\beta \approx 32°$, $\gamma = 0°$).

#243212 Received 17 Jun 2015; revised 30 Jul 2015; accepted 12 Aug 2015; published 10 Sep 2015

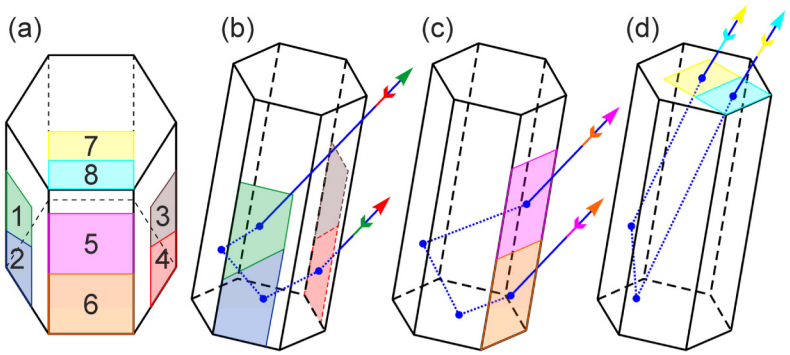

Fig. 2. Skew (1-4) and straight (5-8) plane-parallel beams giving predominant contributions to backscatter. Their ray trajectories are shown in Fig. 2(b) and Figs. 2(c) and 2(d), respectively.

In the physical-optics approximation, if several plane-parallel beams emitted from a finite domain propagate in the backward direction $\theta = 0$, in the wave zone of this domain they produce the diffraction or backscattering peak of the angular radius

$$\theta_{dif} \approx \lambda / A, \tag{7}$$

where A is the typical transversal size of the beams. The phase shifts among these beams can be either chaotic or regular. In the case of chaotic phases, the beams can be summarized incoherently, i.e. these are their Mueller matrixes including the differential scattering cross sections that should be added. If the phase shift among the beams is regular, such beams should be added coherently by summation of their 2×2 scattering or Jones matrixes. Then the Mueller matrix of the total field is found by use of the well-known transformation equations. For the coherent addition, the backscattering peak of Eq. (7) should be cut up by interference spots. The angular scale of the interference spots is equal to

$$\theta_{int} \approx \lambda / B, \tag{8}$$

where $\theta_{int} < \theta_{dif}$ and B is a typical distance between the centers of the coherent beams. The diffraction θ_{dif} and interference θ_{int} angles are the main parameters characterizing the backscatter in this paper.

For the beginning, consider the skew beams at the fixed column orientation of ($\beta = 32.22°$, $\gamma = 0°$) where their contributions to the backscatter is maximal. Here phases of the beams are the same because of similarity of their ray trajectories. Therefore contributions of the beams to the backscatter should be summarized coherently, i.e. by summation of their 2×2 Jones matrixes. The Jones matrixes of the beams 1-4 at this column orientation though approximately but with high accuracy of about 5% [5] are equal to

$$\mathbf{J}_1 = -\mathbf{J}_2 = -\mathbf{J}_3 = \mathbf{J}_4 = q\begin{pmatrix} 0 & 1 \\ -1 & 0 \end{pmatrix}, \tag{9}$$

where $|q| \approx 0.8$. The matrix of Eq. (9) means that if incident light is linearly polarized, the scattered light is linearly polarized, too, but its polarization direction turns out to be perpendicular. This phenomenon is caused by two total internal reflections of the ray trajectory of Fig. 2(b) inside the crystal.

Also, in Eq. (9) we see that the mirror-symmetric beams 1-3 and 2-4 are in antiphase. It follows from the summation of the corresponding pairs of the Jones matrixes $\mathbf{J}_1 + \mathbf{J}_3 = \mathbf{J}_2 + \mathbf{J}_4 = 0$. Thus, we obtain that the energy delivered to the backward direction

#243212 Received 17 Jun 2015; revised 30 Jul 2015; accepted 12 Aug 2015; published 10 Sep 2015

from, say, the beams 1 and 3 is eliminated because of interference between them. If energy of two beams is eliminated in the point $\theta = 0$ because of interference, this interference should

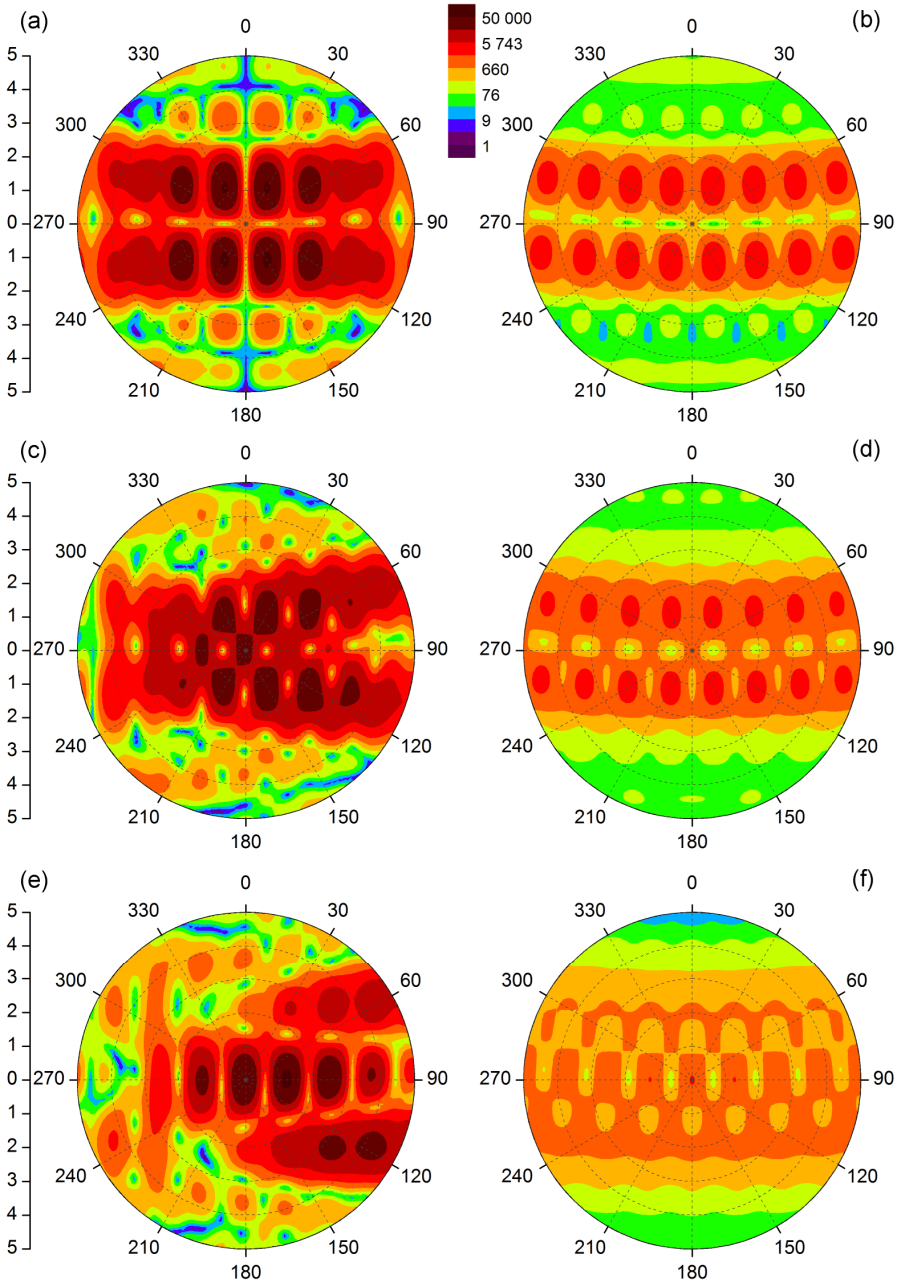

Fig. 3. The differential scattering cross section of the skew beams 1-4 within the cone of 5° for the regular and irregular columns at $\lambda = 0.532\,\mu m$. The left patterns correspond to the columns with the distortion angles: $\xi = 0°$ (a); $\xi = 0.2°$(c); and $\xi = 0.5°$(e) at the fixed orientation ($\beta = 32.22°$, $\gamma = 0°$) while the patterns averaged over the rotation angle γ are shown to the right.

#243212 Received 17 Jun 2015; revised 30 Jul 2015; accepted 12 Aug 2015; published 10 Sep 2015

increase the backscattered light in some neighbor points $\theta \neq 0$ where the beams become in phase.

These regularities are shown in Fig. 3(a) where the differential scattering cross section of these four beams $\sigma(\theta,\varphi)$ is calculated within the angular radius of 5° around the backward direction $\theta = 0$ for the given column orientation and wavelength of $\lambda = 0.532\,\mu\text{m}$. Assuming the typical size of the beams as $A \approx D/3 \approx 10\,\mu\text{m}$ we obtain that the diffraction angle is $\theta_{dif} \approx 3°$ at $\lambda \approx 0.5\,\mu\text{m}$. Figure 3(a) illustrates that the main energy of the scattered light is concentrated roughly within the cone of $\theta < 3°$. In the backward direction $\theta = 0$, intensity of the scattered light reveals a deep minimum that is explained above by the destructive interference.

As for the interference angle defined by Eq. (8), we assume $B \approx D$ that results in $\theta_{int} \approx 1°$. In Fig. 3(a) the bright spots near the backward direction of the angular size of about 1° are just the interference spots where all four beams are in phase producing the constructive interference. Let us remind that in these spots linear polarization is turned perpendicularly relative to linearly polarized incident light that leads to large depolarization ratios.

The interference spots created by the skew beams have also the following remarkable property. These spots prove to be rather steady to crystal rotation about the angle γ. Figure 3(b) shows the value $\sigma(\theta,\varphi)$ averaged over such rotation. We see that Figs. 3(a) and 3(b) have the same angular structure. This steadiness of the interference spots is explained by relatively small change of distance B between the beams on the particle surface during rotation taking into account that the contribution of the scattered beams to the backscatter is essential only for rather small rotation angles γ.

The backscatter properties caused by the straight beams, say, 5-6 are more trivial. Indeed, at the given orientation of ($\beta = 32.22°$, $\gamma = 0°$) these beams have the same phase and they are in contact with each other forming one more large beam. The differential scattering cross section of the beams 5-6 is reduced to the diffraction pattern of their combined rectangular beam that is shown in Fig. 4(a). We note that Fig. 4(a) could be also obtained by summation of two separate diffraction patterns of the beams 5 and 6 plus the interference term between them. Since the ray trajectories of the straight beams at the given particle orientation are planar, their Jones matrix is diagonal resulting in very small magnitudes of the depolarization ratio in the backward direction. An averaging over the rotation angle γ shown in Fig. 4(b) only smooth the angular structure of Fig. 4(a) unlike the case of the skew beams.

5. Backscattering peak for the randomly oriented irregular columns

Taking into account the physical regularities discussed in the previous section, in this section we study the desired impact of the shape distortion of the columns on their backscattering properties at random particle orientation. It is obvious that the phase shifts among three groups of the beams 1-4, 5-6 and 7-8 are chaotic because of the condition $D << \lambda$. Therefore we can add these beam groups incoherently by summation of their Mueller matrixes

$$\mathbf{M} = \mathbf{M}_{skw} + \mathbf{M}_{str}^{(5,6)} + \mathbf{M}_{str}^{(7,8)}. \qquad (10)$$

It is worthwhile to note that anyone could solve the strict problem of light scattering by a column of the given diameter $D = 30\,\mu\text{m}$ at any particle orientation by use of the Maxwell equations. Such a strict solution includes automatically all interference terms. However, consider, for example, the interference term between a skew and straight beams. For a fixed particle orientation, this term is a quickly oscillating quantity depending on small deviations of particle sizes. Indeed, if the diameter D is mentally changed to, say, $D + \lambda/2$, this

#243212 Received 17 Jun 2015; revised 30 Jul 2015; accepted 12 Aug 2015; published 10 Sep 2015

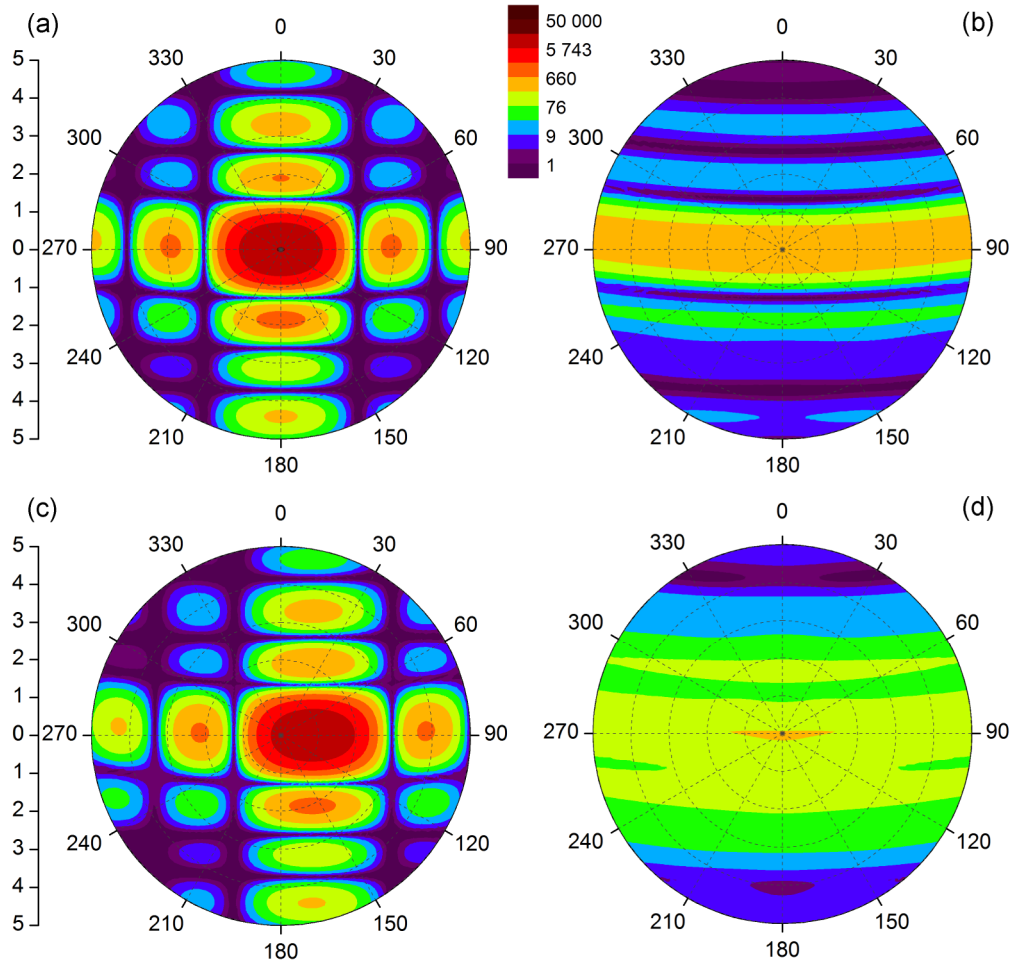

Fig. 4. The same as Fig. 3 for the straight beams 5-6 where Figs. 4(a,b) and 4(c,d) correspond to the regular ($\xi = 0°$) and irregular ($\xi = 0.5°$) columns, respectively.

procedure changes the phase shift between the beams on the quantity comparable to π that results in the opposite sign of the interference term. Consequently, such interference terms have no physical meaning; these terms are eliminated during any averaging over particle sizes. The approximation defined by Eq. (10), on the contrary, is justified from the physical point of view since it excludes such quickly oscillating interference terms in advance.

Figure 5 shows the differential scattering cross section $\sigma(\theta)$ for the randomly oriented regular and irregular columns calculated in both the geometric-optics and physical-optics approximations. Let us begin with the geometric-optics values. We see that the regular column creates the singularity like $1/\theta$ because of the corner-reflection effect as it was described in details earlier [4]. As for the irregular columns, it is obvious that at the fixed column orientation ($\beta \approx 32°$, $\gamma = 0°$) any shape distortion violating the dihedral angle of 90° shifts the scattering directions of all 8 beams from the backward direction $\theta = 0$ to its vicinity $\theta \neq 0$. Moreover, we proved that it was impossible to return the beams to the backward direction by a change of particle orientations. Therefore we watch in Fig. 5 that the shape distortion has replaced the singular peak of the backward direction by some regular functions $\sigma(\theta)$ which have a gap at the backward direction, the angular radius of this gap being about the distortion angle ξ.

#243212 Received 17 Jun 2015; revised 30 Jul 2015; accepted 12 Aug 2015; published 10 Sep 2015

In the physical-optics approximation, the geometric-optics gap and peaks have been smoothed as it is presented by the solid curves. We obtain that these curves distinctly reveal the backscattering or diffraction peak which outspreads roughly until the diffraction angle θ_d. Beyong the diffraction peak $\theta > \theta_d$, the geometric-optics and physical-optics functions $\sigma(\theta)$ practically approach each other. Thus, the backscattering peak of the angular radius of about θ_d exists for the shape-distorted crystals as well. However, the amplitude of this backscattering peak strongly decreases with the distortion angle ξ as seen in Fig. 5. As a result, we conclude that the backscattering peak practically disappears if the distortion angle exceeds the diffraction angle: $\xi > \theta_{dif}$.

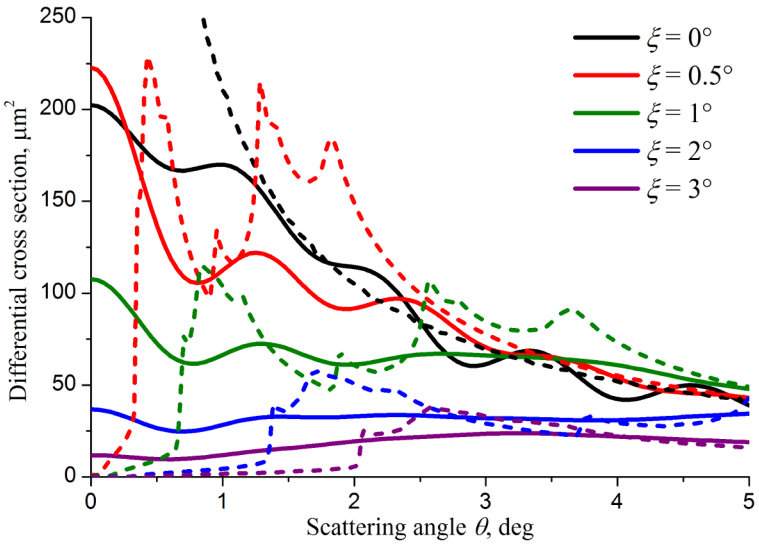

Fig. 5. The differential scattering cross sections for the randomly oriented regular and irregular columns calculated in the geometric-optics (dashed) and physical-optics (solid) approximations.

Also, the physical-optics values $\sigma(\theta)$ in Fig. 5 reveal strong oscillations relative to the scattering angle θ with the scale of about θ_{int}. These oscillations are the interference rings caused by interference among the skew beams 1-4. A proof of this statement follows from Fig. 6 presenting the differential scattering cross section $\sigma_{skw}(\theta)$ for only the skew beams. We see in Fig. 6 that this is the destructive interference of the beams 1-4 taking place for the regular column that produces a deep valley in the cone of $\theta < \theta_{int}$. An increase of the distortion angle from $\xi = 0°$ to $\xi \approx 0.6°$ replaces this interference dark spot around the backward direction by the bright interference spot. Then, at $\xi \to \theta_{dif}$, the bright interference spot is decreased accompanying the dissipation of the diffraction peak.

#243212 Received 17 Jun 2015; revised 30 Jul 2015; accepted 12 Aug 2015; published 10 Sep 2015

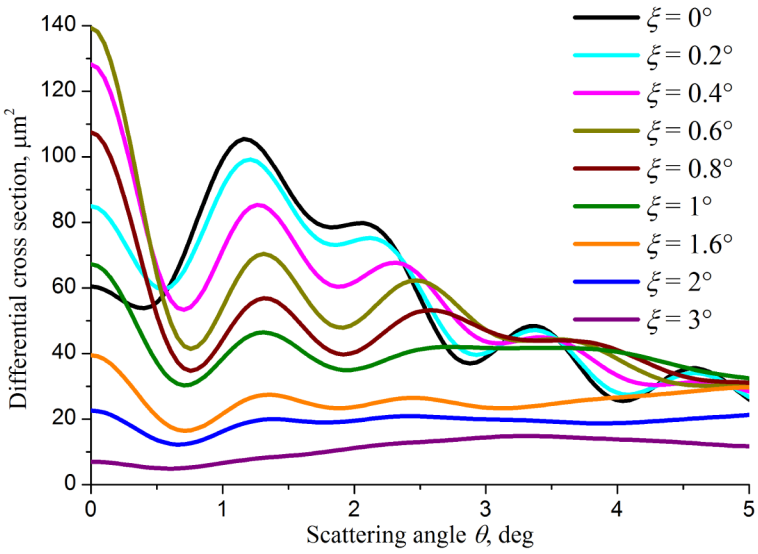

Fig. 6. The same as Fig. 5 for the skew beams 1-4 only.

These conclusions can be also visualized by use of Figs. 3(b), 3(d), and 3(f). Indeed, our numerical calculations show that the patterns of Figs. 3 and 4 are not qualitatively changed for those magnitudes of the tilt angle β which give essential contributions to the backscatter. Therefore a mental rotation of the patterns of Figs. 3(b), 3(d), and 3(f) around their centers corresponds approximately to the desired averaging over random orientation. Such mental rotation of the figures gives approximately the functions $\sigma_{skw}(\theta)$. It is seen from Fig. 3(b) that the dark interference ring appears around the backward direction because of the destructive interference explained above. Then, at $\xi = 0.2°$ and $\xi = 0.5°$, the dark interference ring is replaced by the bright interference rings according to Figs. 3(d) and 3(f).

The same rotation of the patterns of Figs. 4(b) and 4(d) shows that the differential scattering cross sections for straight beams $\sigma_{str}(\theta)$ are monotonically decreasing functions of the scattering angle. Thus, the total differential scattering cross section $\sigma(\theta)$ of Fig. 5 oscillates slower than Fig. 6 because of the addition of these functions $\sigma_{str}(\theta)$.

Several polarization elements of the Mueller matrix of Eq. (1) calculated for the irregular crystals in the physical-optics approximation are shown in Fig. 7. Here we watch the same strong impact of the shape distortion on the polarization elements of the Mueller matrix. These elements oscillate relative to the scattering angle with the scale of about θ_{int} like the first element $\mathbf{M}_{11}(\theta) = \sigma(\theta)$. Instead of the element $m_{33}(\theta)$, Fig. 7(d) shows the depolarization ratio defined by Eq. (6). The other elements are small and they are not presented here.

6. Backscatter ratios for the randomly oriented irregular columns

The angular structure of the backscattering peak of the width of several degrees can be of interest only for passive remote sensing of cirrus clouds by means of radiometers measuring the Mueller matrix in wide angular interval. However, such a wide peak has no practical applications to lidar signals. Indeed, a lidar with the receiver of the diameter, say, 1 m detects the light that is backscattered by a crystal in the cone of the angle $1\,\text{m}/10\,\text{km} = 10^{-4} \approx 0.006°$ if the crystal is localized at the height of 10 km. Consequently, only the Mueller matrix of

#243212 Received 17 Jun 2015; revised 30 Jul 2015; accepted 12 Aug 2015; published 10 Sep 2015

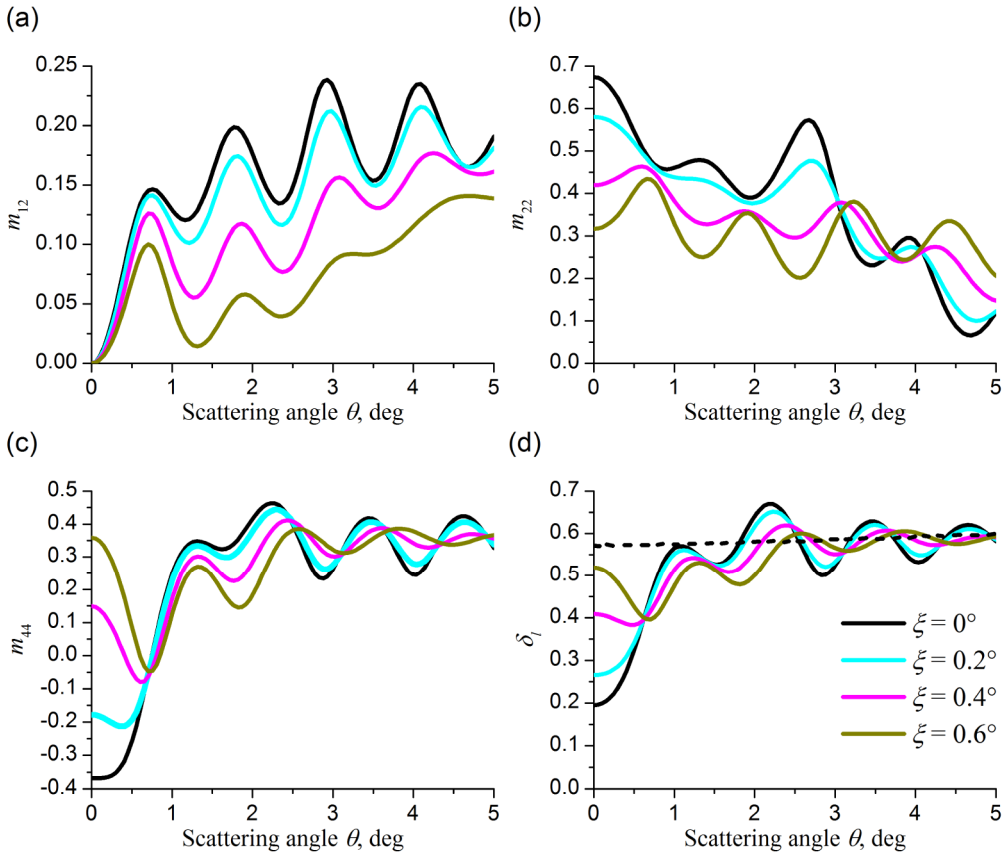

Fig. 7. Polarization elements of the Mueller matrix (a-c) and the linear depolarization ratio (d) for the regular and irregular columns. In Fig. 7(d), the dotted line corresponds to the geometric-optics approximation.

Equation (2) including the backscattering cross section $\sigma(0)$ are important for interpretation of lidar data.

The backscattering cross section $\sigma(0)$ for two wavelengths of 0.532 μm and 1.064 μm is shown in Fig. 8(a). We see that there are the distortion angles where the backscattering peak is dissipated at the shorter wavelength and it is not dissipated at the longer wavelength. As a result, the color ratio increases as it is presented in Fig. 8(b). The linear depolarization ratio presented in Fig. 8(c) also increases with the distortion angle. This increase is explained by the enlargement of the ratio $\sigma_{skw}(0)/\sigma_{str}(0)$ caused by the replacement of the dark interference spot by the bright one. Such change of the depolarization ratio is also demonstrated in Fig. 7(d) at $\theta = 0$. The increasing lidar ratio in Fig. 8(d) results directly from Fig. 8(a).

As was emphasized above, the model of crystal shape distortion used in this paper is justified neither experimentally nor theoretically. Consequently, the data obtained in this paper are not directly applicable to experimental data. Moreover, we restricted ourselves by the hexagonal column of the fixed diameter of $D = 30\mu m$. Consequently, only the tendencies in the optical properties of cirrus caused by crystal shape distortions, which are obtained in the paper, can be compared with the experimental data. In its turn, the available experimental data reveal great variability caused by large diversity of sizes, shapes and spatial orientations

#243212 Received 17 Jun 2015; revised 30 Jul 2015; accepted 12 Aug 2015; published 10 Sep 2015

of ice crystals occurring in the atmosphere. Moreover, multiple scattering of light in cirrus should be taken into account to retrieve the backscatter ratios.

Taking into account these stipulations, it is interesting to compare the data presented in Fig. 8 with the experimental data that can be roughly taken as $\delta_l \approx 0.4$ [15–18], $L \approx 30$ [15,18], and $\chi \approx 0.8$ [19]. We see that these experimental data are best suited to our backscatter ratios of Fig. 8 if the ice hexagonal column is assumed to be irregular with the distortion angle of $\xi \approx 1°$.

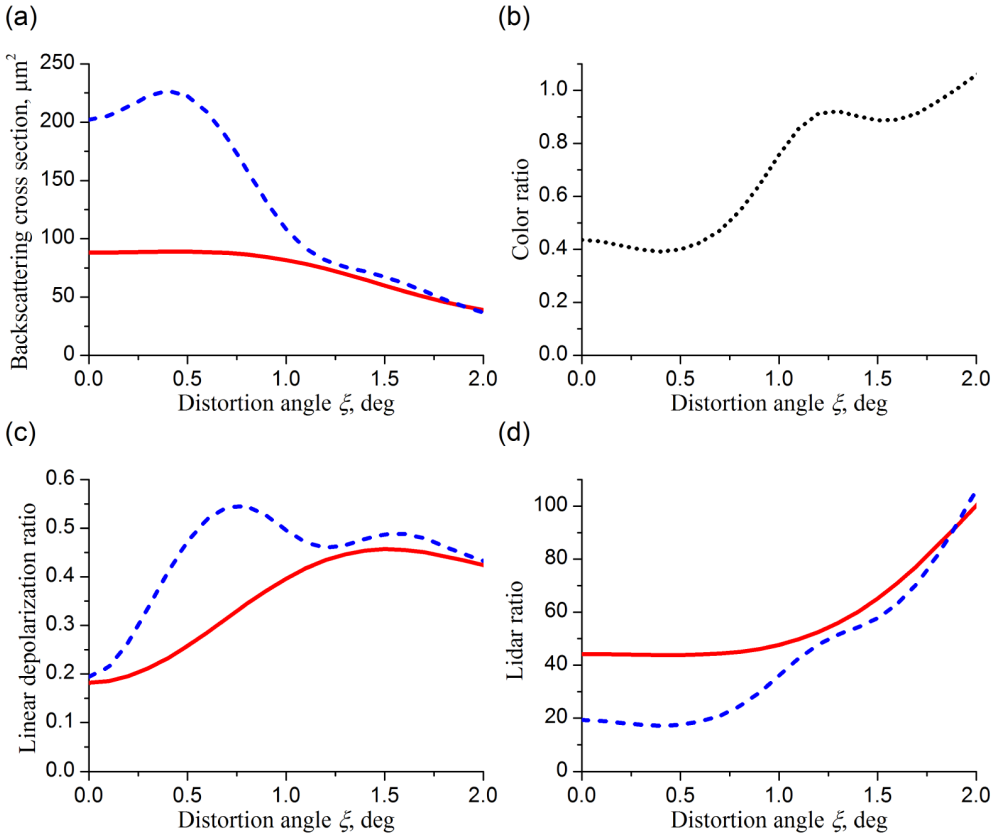

Fig. 8. Backscattering cross sections (a) and the backscatter ratios (c-d) for the randomly oriented column versus its distortion angle calculated in the physical-optics approximation for two wavelengths of 0.532 μm (dashed) and 1.064 μm (solid).

As for numerical calculations of the backscatter in cirrus, we have to distinguish the recent paper by Zhou and Ping [24] which is close to our paper. In [24], the authors simulated the phase function $P(\theta)$ corresponding to our differential scattering cross section of Eq. (1) by use of their IGOM (improved geometric-optics method) algorithm. Their simulation did not find the backscattering peak unlike our physical-optics algorithm which predicts this peak for arbitrary large magnitudes of the size parameter D/λ [26, 27]. Nevertheless, Zhou and Ping proposed to add a backscattering peak to the IGOM phase function. This additional term was obtained from their simulations of the phase functions by use of the PSDT and II-TM algorithms for randomly oriented regular, shape-distorted, and roughened hexagonal ice columns of the moderate size parameter of, say, $D/\lambda < 20$. Then these numerical data revealing the backscattering peak were empirically adjusted by their Eq. (1) for the amplification factor $\zeta(\theta) = P(\theta)/P(5°)$ as $\zeta(\theta) \approx 1 + 0.7[\sin(2\pi\theta D/\lambda)/(2\pi\theta D/\lambda)]$. We note that the authors of [24] concluded that the phase function at the backward

#243212 Received 17 Jun 2015; revised 30 Jul 2015; accepted 12 Aug 2015; published 10 Sep 2015

direction $\theta = 0°$ does not depend of the column size while our physical-optics code predicts such dependence. This disagreement between the qualitative conclusions can be explained by the different averaging procedures used. In this paper, we average the scattered light only over particle orientation at the fixed crystal shape while the additional averaging over crystal shapes for the shape-distorted crystals is taken in [24]. As for the regular columns, a comparison between the data fails since Fig. 1(b) in [24] shows only the normalized quantity. So, the further calculations could clarify this discrepancy. Nevertheless, some qualitative conclusions coincide in [24] and the present paper. Namely, the angular width of the backscattering peak is inversely proportional to the size parameter. It is also interesting to note that the amplification factor at the exact backward direction $\zeta(0°) \approx 1.7$ of the paper [24] corresponds to our irregular crystal with the distortion angle of $\xi \approx 1°$ according to Fig. 5.

7. Conclusions

The physical-optics approximation was previously applied to study the backscattering properties of the pristine hexagonal ice columns and plates of cirrus clouds [26, 27]. We were able to ascertain that the backscatter ratios calculated for the randomly oriented hexagonal columns did not match well with the available experimental data.

Therefore, in this paper, we have studied the impact of shape distortions of a hexagonal ice column on its backscattering properties at random particle orientation by use of the simplest geometrical model of the shape distortion. It is obtained that the backscattering peak around the backward direction previously known for the regular crystal shapes exists for the shape-distorted crystals as well. It spreads from the backward direction until the so-called diffraction angle $\theta_d \approx 3\lambda / D$. However, this peak is dissipated for large shape distortions under the condition $\xi > \theta_{dif}$ where ξ is the distortion angle.

Within the backscattering peak, all elements of the Mueller matrix including the differential scattering cross section, as functions of the zenith scattering angle, undergo oscillations with the angular scale of about the interference angle $\theta_{int} \approx \theta_{dif} / 3$. It is proved that these oscillations are caused by interference of four skew beams. At the exact backscattering direction $\theta = 0°$, this interference is destructive for the regular crystal $\xi = 0°$. Then it becomes constructive for the irregular crystals at $\xi > \theta_{int} / 2$.

The backscatter ratios needed for interpretation of lidar signals are firstly calculated as functions of the distortion angles. These results can explain the inconsistencies between the theoretical and experimental data.

Acknowledgments

This work is supported by the Russian Foundation for Basic Research under Grants no. 15-05-06100 and no. 15-55-53081, by the RF President grant on the support of leading scientific schools NSH-4714.2014.5, by the RF President grant MK-6680.2015.5, by the RF Ministry of Education and Science under the program rising competitiveness of the TSU and supported in part by the Russian Science Foundation (Agreement no. 14-27-00022).

#243212 Received 17 Jun 2015; revised 30 Jul 2015; accepted 12 Aug 2015; published 10 Sep 2015